https://doi.org/10.1016/j.tsf.2023.139920
This is the Pre-Published Version.

Quantitative characterization of thin-film cracking behavior enabled by one-step asymmetrical bending

Hong Hu[1], Ziran Wang[1], Yufeng Luo[1], Pengwei Wang[1], Yaokang Zhang[1], Qiyao Huang[1,*], Zijian Zheng[1,2,3,4,*]

[1]Laboratory for Advanced Interfacial Materials and Devices, School of Fashion and Textiles, The Hong Kong Polytechnic University, Hong Kong SAR, China

[2]Department of Applied Biology and Chemical Technology, Faculty of Science, The Hong Kong Polytechnic University, Hong Kong SAR, China

[3]Research Institute for Intelligent Wearable Systems (RI-IWEAR), The Hong Kong Polytechnic University, Hong Kong SAR, China

[4]Research Institute for Smart Energy (RISE), The Hong Kong Polytechnic University, Hong Kong SAR, China

*Corresponding author: [Qiyao Huang, qi-yao.huang@polyu.edu.hk; Zijian Zheng, tczzheng@polyu.edu.hk]

ABSTRACT

Quantitative characterization of crack behavior in thin-film materials is a fundamental issue in solid mechanics and is of necessity for the development of high-performance flexible electronics. However, such analysis largely relies on the complicated *in-situ* microscopy technique and the operational skills of experienced researchers, thus leading to difficulties in its widespread applications. To address this challenge, we report herein a facile and efficient characterization method based on the asymmetrical bending strategy to achieve the quantitative analysis of the crack

© 2023. This manuscript version is made available under the CC-BY-NC-ND 4.0 license https://creativecommons.org/licenses/by-nc-nd/4.0/

features in thin-film materials without any need for specialized testing instruments. The key to this method is to bend two unparallel edges of the trapezoid-shaped thin film/substrate to form an asymmetrical configuration, in which the local bending radius changes linearly along the bending axis. As such, a large number of bending radii can be achieved on one single sample in one experiment, which significantly simplifies the process of quantitatively relating crack features to mechanical deformation. As a proof-of-concept demonstration, we employ this method for the one-step *in-situ* investigation of the crack behavior of the Cu film on a polymeric substrate.

Keywords: asymmetrical bending, cracking behavior, thin-film, *in-situ* characterization, flexible electronics

1. Introduction

Thin-film materials, such as metals, semiconductors, and ceramics, are widely deposited on deformable substrates for the subsequent fabrication of a variety of flexible electrodes and electronic devices, performing their electronic functions in fields of human-machine interactions [1], energy storage and harvesting [2, 3], sensors [4-6], and smart wearables [7-10]. Since these electronic devices are largely subject to mechanical deformation in use, materials failure may easily occur and one of the failure modes is crack [11-13]. Even cracks initiate and propagate at the microscale, the performance of cracked materials, such as the conductivity of metal [14, 15], the mobility of semiconductor [16], and the dielectric property of ceramics [17] will significantly degrade, which may lead to the device failures. As such, many effective strategies have been developed to avoid cracks in the functional materials, enhancing the performance stability of the as-made interconnects,

electrodes, and devices [18-22]. On the other hand, the crack formation is not always an undesirable process. The control of crack formation can be fully utilized for the realization of many advanced applications, such as, film patterning [23, 24], lithography [25], surface-enhanced Raman scattering [26], and ultrasensitive gas [27], strain [28-31], or vibration sensors [32, 33]. Therefore, no matter in what way the crack is considered, i.e., to be inhibited, to be promoted or even to be controlled, a quantitative understanding of crack behaviors of thin-film materials in response to mechanical deformations could greatly favor the design, fabrication, performance evaluation and optimization of the flexible electronic devices.

To date, a general approach to characterize crack behaviors is to observe the evolution of the micro-scale crack patterns on the thin-film/substrate when it is strained by either uniaxially stretching (Fig. 1a) or bending (Fig. 1b). An *in-situ* microscopic technique, using, for example, scanning electron microscopy (Fig. 1c [34]) or optical microscopy [35], is applied to record the key geometrical features of the cracks (e.g., crack density, ρ) as a function of the deformation (usually, applied strain, ε, Fig. 1d). This *in-situ* technique can provide results that are close to the condition where the thin film material undergoes deformation in practice, and therefore, has been widely adopted in the academia [36-42]. Nevertheless, the application of such a quantitative analysis highly relies on the complicated setup of *in-situ* microscopy and the operational skills of experienced researchers, leading to the difficulties in widespread applications. Many researchers, alternatively, carry out a quasi-*in-situ* approach by observing the crack *in-situ* (e.g., in the SEM chamber), while applying the strain to the observed substrate *ex-situ* (e.g., outside of the SEM chamber [38]). Though this quasi-*in-situ* approach does not require a complicated characterization apparatus, tedious and

time-consuming processes for sample preparation are involved: the testing specimen has to be changed into a specific deformation status and then be placed onto the sample stage of the microscopy for crack observation for every deformation condition. Since a large number of data (i.e., ρ vs. ε) for each sample are essentially required to exclude the possibly random factors in cracking, this quasi-*in-situ* approach may not be preferrable for efficiently capturing the crack behaviors of thin-film materials.

To address the trade-off among operational simplicity, observation efficiency, and data accuracy, we report herein a facile and efficient strategy, named asymmetrical bending strategy, for the quantitative characterization of the crack behavior of the thin-film materials on a polymeric substrate. Differing from the typical loading modes in previous studies where two parallel boundaries are uniformly displaced, the thin-film/substrate in the proposed asymmetrical bending mode is bent at two unparallel edges (Fig. 1e). The bent configuration is considered to be asymmetrical because of its only one symmetrical plane (i.e., *zy* plane), which is one less than those in typical loading modes (*zy* and *zx* planes). As such, the bending radius linearly changes along the direction of the bending axis (*y* axis) rather than keeping as a constant value. The corresponding applied strain can be thus easily determined as a function of position. Via the observation of the cracks in different positions, the quantitative relation between crack density and applied strain can be eventually obtained (Fig. 1f). In principle, our method enables a large number of bending radii (continuously changed) in one single sample in one experiment without any complicated testing equipment, which is much more efficient than the quasi-*in-situ* method and can also provide the result as accurate as those obtained by the *in-situ* method. Through the implementation of this

asymmetrical bending strategy, we measured the crack density of the Cu thin films with different film thicknesses as a function of the applied strains. We found that the two length-scale-dependent material properties, i.e., initial defects and yield strength, are competitive in determining the crack resistance of the film.

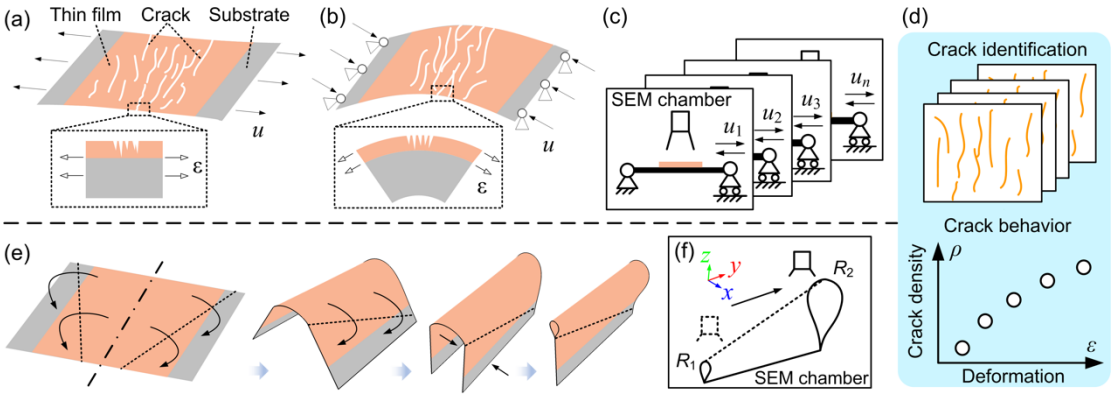

Fig. 1. Schematic illustration of characterization of crack behavior in response to deformation. a) Uniaxially stretching and b) bending can generate a tensile strain on the upper film, thus inducing the cracking. c) *In-situ* test in a SEM chamber. By applying a series of displacements, u, different strains can be applied on the upper film. d) Identification of crack features (crack density, ρ) corresponding to deformation (applied strain, ε) leads to quantitative results of crack behavior (ρ vs. ε data). e) Proposed asymmetrical bending strategy. Two unparallel edges (dotted lines) are bent and approach each other. The local bending radius is not constant, but changes linearly along the bending axis. f) With the observation of cracks on the upper surface at different y positions, the crack behavior can be also obtained quantitatively (the data in d)).

2. Sample preparation and characterization

As a proof-of-concept demonstration, this asymmetrical bending strategy was adopted to study the crack behavior of the ductile Cu thin film on polymeric substrate. The Cu film was thermally evaporated on a 120-μm-thick polyethylene naphthalate (PEN) at 1×10^{-4} Pa vacuum degree with a deposition rate of 0.5 Å/s. Four samples with different film thicknesses of t_f=50 nm, 75 nm, 120 nm and 240 nm were under investigation, which were further confirmed by the SEM cross-sectional

images (Fig. 2). To obtain high-quality cross-sectional views, samples with a notch were fractured in the liquid nitrogen, and then were observed by the field emission scanning electron microscopy (TESCAN, MAIA3, Brno, Czech Republic) with an operation voltage of 25 kV. The surface morphology of the film was characterized by the atomic force microscopy (AFM, XE-100, Park Systems) with the non-contact mode (NCM). The resonance frequency and force constant of the probe in the AFM apparatus (PPP-SEIHR-W, purchased from the NANOSENSORS) were 96-175 kHz and 5-37 N m^{-1}, respectively. The scan rate and Z servo gain for all samples were set as 0.5 Hz and 1.0, respectively. The root mean square (RMS) roughness of the four samples ranged from 0.6-0.8 nm due to the growth of the grain [43], and no texture was observed on the surface (Fig. 3). The crystal structure of the Cu films was analyzed by the X-ray diffraction (XRD) method on the Rigaku Smartlab using Cu Kα radiation (λ=1.546 Å) within 2θ in the range of 5–90°. Fig. 4 shows the XRD patterns of the bare PEN and Cu-coated PEN samples. The peaks of 43.3, 50.4, 74.1, and 89.9°, ascribed to the (111), (200), (220), and (311) crystallographic plane of Cu, demonstrate its polycrystalline Cu phase depositing on the PEN substrate without preferential orientation.

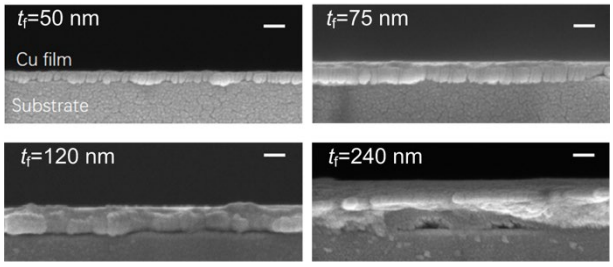

Fig. 2. SEM images showing the cross section of the Cu-film/PEN assembly for t_f=50 nm, 75 nm, 120 nm, and 240 nm, respectively (t_f denotes the film thickness). The scale bars are 100 nm.

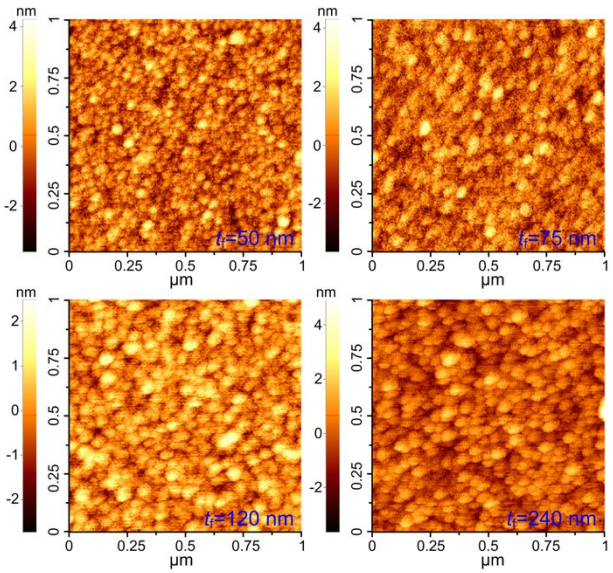

Fig. 3. AFM images showing the surface morphology of the Cu film for t_f=50 nm, 75 nm, 120 nm, and 240 nm, respectively. No obvious texture was found in these Cu films.

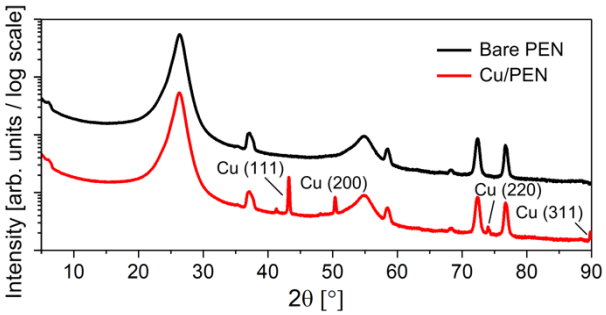

Fig. 4. XRD characterization of bare PEN and Cu-coated PEN (t_f=240 nm) with 5°<2θ<90°. The XRD pattern indicates that the evaporated Cu film is polycrystalline.

3. Results

Based on the neutral plane theory, when a film/substrate assembly (thickness: t) is bent at a specific bending radius (R), the actual strain (ε') applied on the upper film is given by [44]:

$$\varepsilon' = \varepsilon \frac{1+2\eta+\chi\eta^2}{(1+\eta)(1+\chi\eta)} \quad (1)$$

where $\varepsilon = t/2R$ is the applied (nominal) strain that is usually taken as a measure of the deformation, $\eta = t_f/t_s$ is the ratio of the thickness of the deposited thin film materials (t_f) to that of the substrate (t_s), and $\chi = E_f/E_s$ is the ratio of Young's modulus of the film (E_f) to that of the

substrate (E_s). For a thin film case where the thickness of the deposited thin-film material (t_f) is far thinner than that of the substrate (t_s), $\eta \to 0$, Equation (1) reduces to

$$\varepsilon' = \varepsilon \tag{2}$$

Equation 2 relates the applied strain to the actual strain on the material. It indicates that bending a t-thick sample with a bending radius of R could be equivalent to uniaxially stretching it with the strain of $\varepsilon = t/2R$. If Equation 2 cannot be satisfied (e.g., η is not close to 0), a corrective factor has to be introduced to the ρ-ε data to ensure that the crack behavior is comparable with the uniaxial stretching approach.

Therefore, Equation 2 for our strategy needs to be validated before experiments. We established a simple finite element (FE) model, which involved a geometry of an isosceles trapezoid shell part with the height (H), shorter (d_1) and longer (d_2) edges in arb. units. A composite shell section with two plies was adopted to model the thin film/substrate system, where the thickness of the upper and lower ply was 1×10^{-4} and 0.2 arb. units, respectively. All the materials were homogenous, isotropic and linearly elastic. The Young's modulus of the upper ply was 1/50 of the lower one. The geometry was meshed into more than 5000 four-node doubly curved thin shell elements with reduced integration method (S4R). Two unparallel edges were bent along with the y axis at 90° angle, and then approached each other (Fig. 5a). The model was performed in the commercial FE software Abaqus using the standard Newton-Raphson numerical algorithm. Two different radii formed at the two free ends of the shell (i.e., R_1<R_2), leading to the formation of nonuniform actual strain ε', with a maximum strain value at y=0 (R=R_1, Fig. 5b). The local bending radius R was then obtained by fitting the curved cross section with a circle (e.g., y=8, R=1.28, Fig. 5c). We analyzed ε' at the center

of the upper ply (dotted line, Fig. 5b) and R as functions of the y position, and found that, 1) $\varepsilon'=\varepsilon$ still held true (Fig. 5d), and 2) R changed linearly with y (lower inset of Fig. 5d) for different d_1, d_2, and H. Given that H, R_1 and R_2 are all known, one can easily obtain the local ε for an arbitrary y position, and then correspond ε to the crack features, ρ, to quantify the crack behavior. Notably, since the two relationships that $\varepsilon'=\varepsilon$ and that R is linearly related to y are valid with independence of the shell sizes (i.e., d_1, d_2 and H), the sample in experiment can be bent in arbitrary shape. There is no need to constrain any one of the geometrical dimensions in sample preparation, which largely simplifies the experiment especially when a set of samples are under investigation.

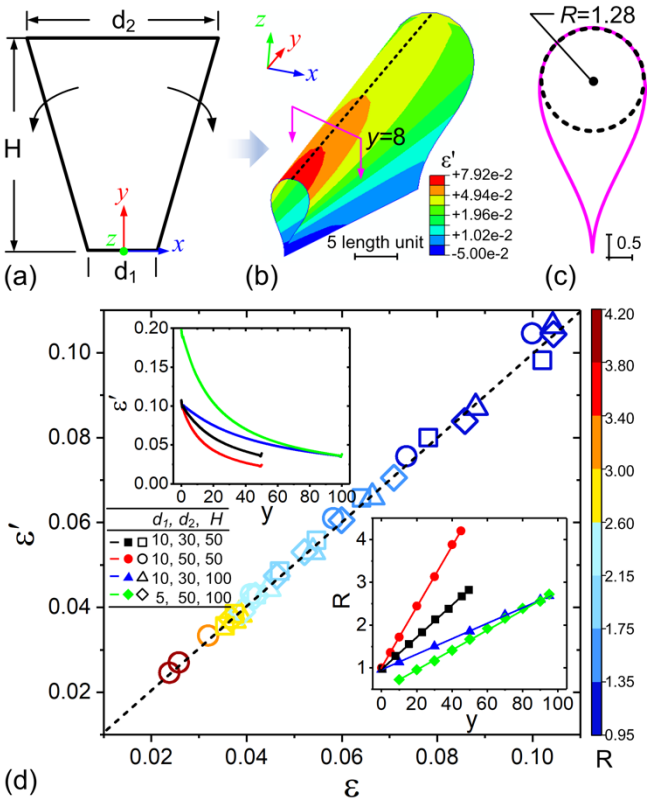

Fig. 5. Finite element (FE) results indicating that Equation 2 is valid for the asymmetrical bending strategy. a) Geometrical model for bending simulation. Two unparallel edges were bent along with the y axis. b) Shape after bending. Two different bending radii form at the two free sides of the bent part with non-uniform actual strain on the upper film (R_1<R_2). c) Curved cross section at the position of y=8. The local bending radius R=1.28 can be estimated by fitting the curve with a circle. d)

Relationship between actual strain ε' and applied strain ε for different d_1, d_2 and H. The dotted line denotes where $\varepsilon' = \varepsilon$. The color of the symbols denotes the R value ranging from 0.95 to 4.2. The upper inset shows the evolution of the non-uniform ε' at the center of the upper ply along the y axis (dotted line in b)). The lower inset shows R as a linear function of y.

Fig. 6a shows a representative sample bent asymmetrically, which only involves a very common foldback clip to fix the two unparallel edges. The inset shows the SEM image of the cross section before bending (t_f=75 nm). For this sample, H, R_1, and R_2 are 2.25 cm, 1 mm, and 1.9 mm, respectively (Figs. 6b and 6c). The surface cracks were observed by SEM, and then the as-captured SEM images were post-processed as described by Talab et al. [45]. Fig. 6d compares the as-captured (upper panel) and post-processed SEM images (lower panel). The good match between them indicates the correctness of our image processing. Fig. 6e displays the evolution of the cracks for different local bending radii. Zigzag cracks propagate along the direction perpendicular to the tensile direction (arrow). With the increase of R from 1.1 mm to 1.85 mm, the number of the cracks, N, which is an average number of the total cracks forming on 25 equally spaced detection lines parallel to the tensile direction within the image width (~55 μm), decreases from N=10.6 to N=0.8. Note that the R or the corresponding ε value for each crack image is approximated as, although strictly not, a constant for simplicity. This approximation does not result in significant error in quantifying the crack behavior, because the change of R within an image is very slight (e.g., from 4.8 % to 4.72 % for the second image in Fig. 6)

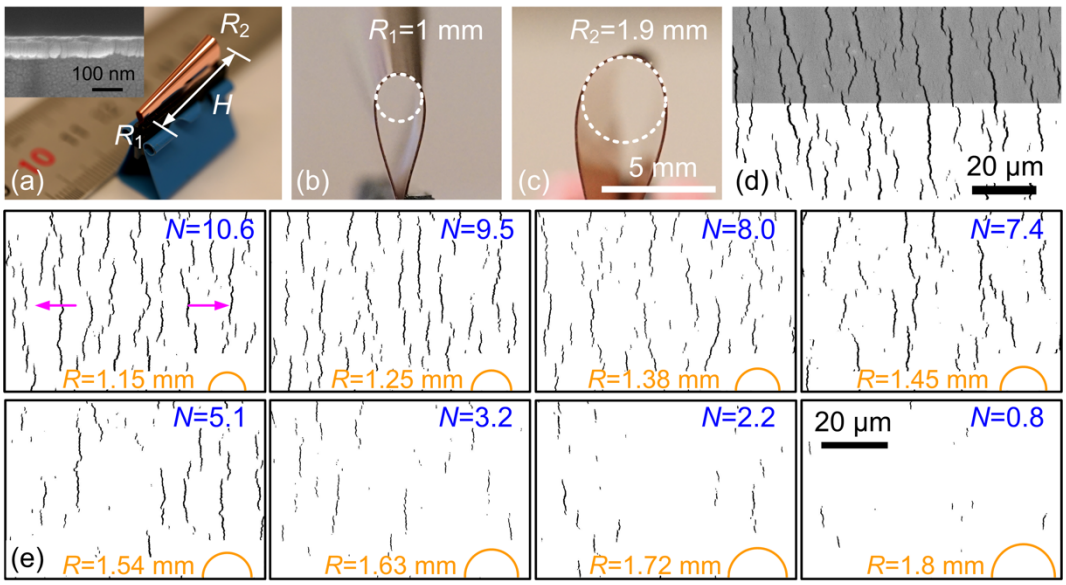

Fig. 6. Representative results showing sample bent asymmetrically and cracks for different bending radii. a) Photograph of a bent sample. Only a very common foldback clip is used to fix the two unparallel edges. The inset shows the SEM image of the cross section. b) and c) Photographs showing R_1=1 mm and R_2=1.9 mm by fitting the curved cross section with a circle, respectively. d) Comparison of as-captured (upper panel) and post-processed SEM image (lower panel) of cracked surface. e) Evolution of cracks as local R changes. The arrows indicate the tensile direction. N is an average number of cracks counted on 25 equally-spaced detection line in the tensile direction. The bottom-right semicircles scale with R ranging from 1.15 mm to 1.8 mm.

We therefore used this method to analyze crack images. Fig. 7 shows the post-processed SEM images of the crack evolution for different Cu film thicknesses (from left to right, t_f=50, 75, 120, and 240 nm, respectively), and local bending radii R. With the increase of t_f, the crack opening increases, while with the increase of R, fewer cracks initiate. Interestingly, the cracks propagate solely without any other obvious crack interactions that may induce different fragmentations of the film, e.g., mid-point cracking, transverse buckling failure, delamination and even dynamic fracture, which were often observed for many inorganic thin films (e.g., SiO_x, ZnO, and ITO) on a polymeric substrate [11, 46-48]. It indicates that the crack behavior of the ductile thin film (Cu) differs

significantly from the brittle one [49], which will be discussed in details latter.

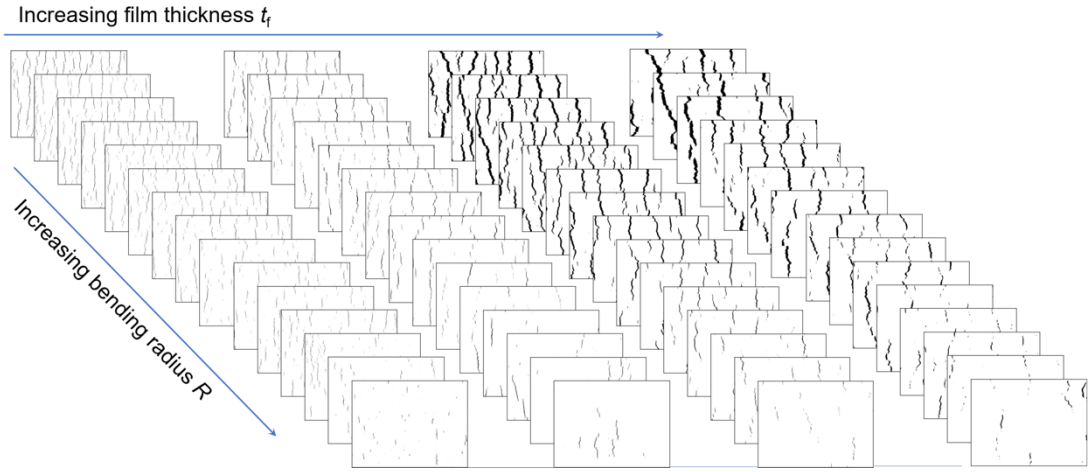

Fig. 7. Post-processed SEM images showing crack evolution for different film thicknesses t_f and local bending radii R. From left to right, t_f=50, 75, 120, and 240 nm, respectively. The size of each image is 52 μm × 45 μm (width × height).

We then performed statistics on the geometrical feature of the cracks. Fig. 8 depicts the crack density ρ as a function of the applied strain ε for different film thickness t_f, where the crack density is defined as the number of cracks (N) per unit length in the tensile direction. The shadow regions denote the standard deviation in averaging N. ρ raises with ε for different t_f. However, the thicker film has smaller crack density at the same strain, and is more likely to reach the saturation state, where no more cracks form as the strain increases (i.e., ρ no longer raises with ε, and e.g., ε>10% for t_f=120 and =240 nm). This result implies the strong thickness dependence of the crack behavior [36].

It should be pointed out that since the strain of an asymmetrically bent sample changes continuously along the bending axis, the crack behavior may be partially the result of the neighboring region that undergoes different strains (or namely, neighboring effect). To address this

issue, we also bent the four samples by the typical bending strategy (Fig. 1b, two parallel edges were loaded, conducted *ex-situ*), and compared the results with those by the asymmetrical one. As shown in Fig. 8a, the ρ *vs.* ε data obtained by these two strategies are very close to each other for different t_f (asymmetrical strategy: solid symbols; typical strategy: open symbols). Furthermore, the cracks also show nearly the same patterns for different t_f and ε (SEM images, Fig. 8b). These results demonstrate that the asymmetrical strategy can exactly lead to the same crack behavior as the typical one. Note that our experiments cannot exclude the possible neighboring effect on the characterization of thin film cracking. This effect may be important in the certain material behavior that shows strong dependence on the strain distribution (e.g., abnormal grain growth in metal films [50]), but is negligible in our bending strategy, which aims at presenting the ρ-ε data.

The critical strain of a thin film material, ε_c, defined as the strain for the crack initiation, can be further estimated by extrapolating the ρ-ε data back to ρ=0 (Experimental details of this method for determining the critical strain can be found in Ref. [38]). The inset of Fig. 8a shows ε_c as a function of t_f. ε_c first increases (t_f<120 nm), and then nearly unchanged (t_f>120 nm) with the increase of t_f. This result indicates that the strength of the Cu film can be enhanced by increasing the film thickness, while this enhancement may disappear for very thick film, which is in good agreement with the experiments reported by Kim et al. [51].

It is also noted that our experimental results are different from those by some other researchers, e.g., Zhao et al. [52], Peng et al. [39], and Mora et al. [53]. In these studies, the thicker film is found to be easier to initiate the cracks than the thinner one, i.e., the larger t_f leads to the smaller ε_c. This

contradiction on the thickness dependence of critical strain is not surprising, because the Cu film in this study and also in those by Lu et al. [36], Niu et al. [38], and Kim et al. [51] are ductile material, while the materials in the Refs. [39, 52, 53] are highly brittle. The brittle material behaves without any important yielding or plastic deformation even at the failure strain, thus can be approximately considered linearly elastic. For the ductile material, however, the strong material nonlinearity due to the strain hardening ability has to be taken into account.

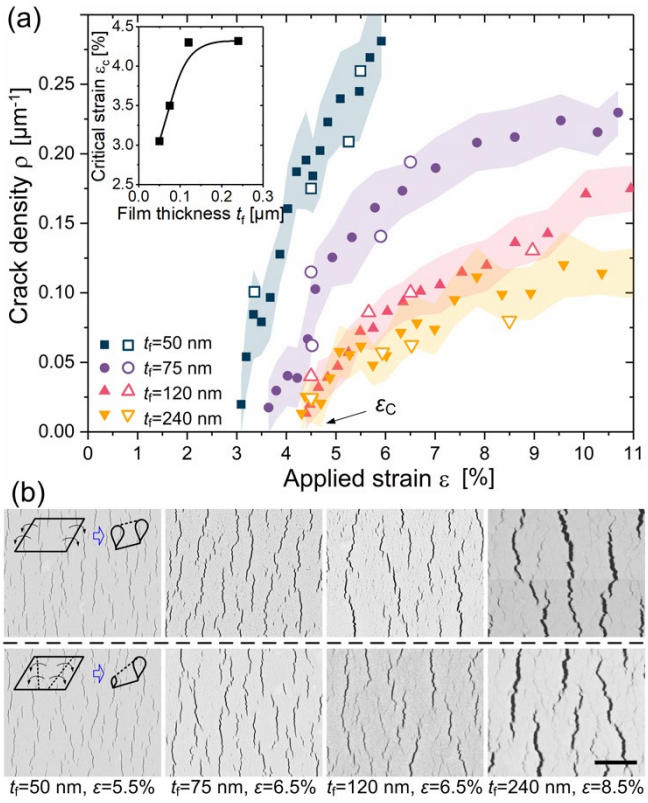

Fig. 8. a) Experimental results of crack density ρ as functions of applied strain ε for Cu film with different thicknesses t_f on PEN by asymmetrical (solid symbols) and typical bending strategies (open symbols). The critical strain, ε_c, defined as the strain for crack initiation, can be estimated by extrapolating the ρ-ε data back to ρ=0. The inset shows ε_c as a function of t_f. b) Comparison of crack patterns by the typical (upper panel) and the asymmetrical (lower panel) strategies for different film thicknesses t_f, and different bending strains ε, respectively. The scale bar is 10 μm. The results demonstrate that these two strategies exactly lead to the same ρ-ε data and crack patterns.

4. Discussion

For a better understanding of the role of material nonlinearity in the crack behavior of the Cu film, we measured the morphology of cracked surface by AFM (ε=5%, Fig. 9a). With the increase of the film thickness, both the depth and width of the cracks under the same strain increase, which is in consistent with the results by Park et al. [54]. The surface profile near the cracks is not horizontal, but show a slope instead (Fig. 9b). As the slopes at the two sides of the cracks are symmetrical about the valleys, the sloped profiles should not result from the possible levelling error of the sample stage. Actually, the sloped profiles imply the ductile fracture mechanism of the Cu film. Before the formation of a channel crack, large scale plastic deformation is accumulated near somewhere with strain localization. In this process, a traction due to the film necking may exceed the adhesion, and thus cause the interfacial debonding, which, as positive feedback, promotes the necking of the film [36, 55]. As a result, a thinned zone symmetrically presents at the two sides of the crack (called plastic zone, the inset in Fig. 9b).

Knowledge of this ductile fracture mechanism allows us to explain the correlation between the strength of ductile thin film material (e.g., Cu here) and film thickness. Regarding the length scale dependence of material properties, thicker film could generally have more initial defects (e.g., voids and dislocation of grain boundaries [56, 57]), and thus shows a lower material strength with smaller crack resistance to the strain. However, the increase of film thickness can additionally lead to the decrease of the yield strength for a ductile material because of the growth of the grain size [36]. Material with lower yield strength exerts a weaker traction in the necking process. The positive feedback is thus weakened and the crack initiation delays [58]. In other words, the initial defects

and yield strength of the material are competitive with each other in determining the crack resistance of a ductile thin film material on substrate. According to our experiments (see Fig. 8), with the increase of film thickness, the reduction of the yield strength may dominate the enhancement of the material strength for small t_f, while on the contrary, i.e., large t_f, the statistical effect of initial defects becomes so important that this enhancement tends to disappear.

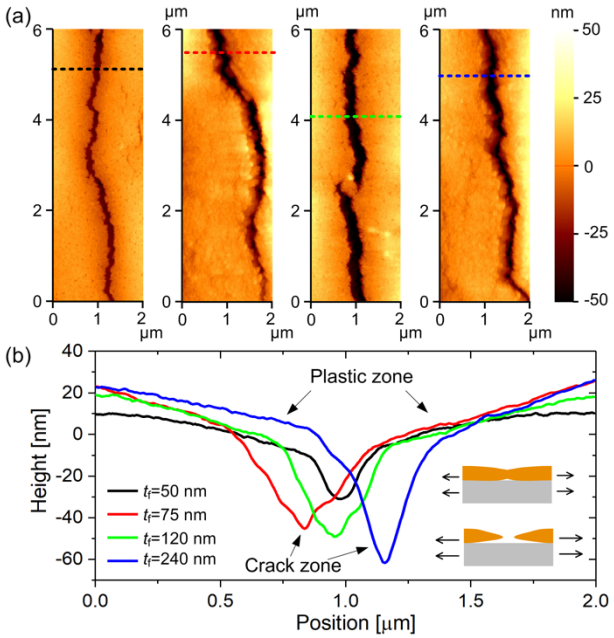

Fig. 9. Evidence for ductile fracture mechanism of Cu film. a) AFM images showing surface morphology near the crack tip for different film thickness, from left to right, t_f=50, 75, 120 and 240 nm, respectively. b) Surface profile measured at the position coded with dotted lines in a). Near the cracks, the profiles present slopes, indicating the plastic zone here due to the typical necking process of a ductile material. The inset illustrates the development of a crack in a ductile thin film material by tensile load.

5. Conclusions

In summary, we developed an asymmetrical bending strategy to enable the efficient and quantitative characterization of the crack behavior of the thin-film/substrate. This strategy, by bending two unparallel edges, leads to the local bending radius as a linear function of the position

along the bending axis. The main advantage of our strategy is that the continuously changed bending radius (i.e., continuous deformation degree), in principle, can be achieved by a single experiment in a single sample without any complicated *in-situ* tester, thus largely fascinating the sample preparation and crack characterization. As a proof-of-concept demonstration, we studied the crack behavior of Cu film with different thicknesses on PEN substrate. We found that two length-scale-dependent material properties, i.e., initial defects and yield strength, may be competitive in determining fracture mechanism and the crack resistance to strain of the ductile materials. We believe that such a one-step investigation approach enabled by asymmetrical bending strategy could further benefit the in-depth understanding on the electrical performance of the thin film materials and devices associated with their mechanical deformations.

Acknowledgements

We acknowledge the financial support from the RGC Senior Research Fellowship Scheme (SRFS2122-5S04), the General Research Fund of Hong Kong (15212021), and the Hong Kong Polytechnic University (1-ZVQM, 1-CD44, and 1-ZVT8). We also acknowledge the use of the faculties in Research Facility in Materials Characterization and Device Fabrication (UMF) at the Hong Kong Polytechnic University.

Author contributions

Hong Hu: Conceptualization, Methodology, Software, Validation, Formal analysis, Investigation, Visualization, Writing - Original Draft, Writing - Review & Editing

Ziran Wang: Methodology, Validation, Formal analysis, Investigation, Resources

Yufeng Luo: Methodology, Validation, Investigation

Pengwei Wang: Methodology, Validation, Investigation

Yaokang Zhang: Methodology, Validation

Qiyao Huang: Conceptualization, Methodology, Writing - Review & Editing, Funding acquisition

Zijian Zheng: Conceptualization, Methodology, Writing - Review & Editing, Supervision, Funding acquisition

Competing interests

The authors declare no competing interests.

Data availability

The data that support the findings of this study are available from the corresponding author upon reasonable request.

References

[1] J. Park, D.-h. Kang, H. Chae, S.K. Ghosh, C. Jeong, Y. Park, S. Cho, Y. Lee, J. Kim, Y. Ko, J.J. Kim, H. Ko, Frequency-selective acoustic and haptic smart skin for dual-mode dynamic/static human-machine interface, *Sci. Adv.* 8 (2022) eabj9220. https://doi.org/10.1126/sciadv.abj9220.

[2] Y. Li, Y. Zhang, J. Yi, X. Peng, R. Cheng, C. Ning, F. Sheng, S. Wang, K. Dong, Z.L. Wang, Large-scale fabrication of core-shell triboelectric braided fibers and power textiles for energy harvesting and plantar pressure monitoring, *EcoMat* 4 (2022) e12191. https://doi.org/10.1002/eom2.12191.

[3] Y. Zhang, X. Guo, J. Huang, Z. Ren, H. Hu, P. Li, X. Lu, Z. Wu, T. Xiao, Y. Zhu, G. Li, Z. Zheng, Solution process formation of high performance, stable nanostructured transparent metal electrodes via displacement-diffusion-etch process, *npj Flex. Electron.* 6 (2022) 4. https://doi.org/10.1038/s41528-022-00134-2.

[4] H. Hu, D. Wang, H. Tian, Q. Huang, C. Wang, X. Chen, Y. Gao, X. Li, X. Chen, Z. Zheng, J. Shao, Bioinspired Hierarchical Structures for Contact-Sensible Adhesives, *Adv. Funct. Mater.* 32 (2022) 2109076. https://doi.org/10.1002/adfm.202109076.

[5] X. Wei, H. Li, W. Yue, S. Gao, Z. Chen, Y. Li, G. Shen, A high-accuracy, real-time, intelligent material perception system with a machine-learning-motivated pressure-sensitive electronic skin, *Matter* 5 (2022) 1481-1501. https://doi.org/10.1016/j.matt.2022.02.016.

[6] Y. Zhang, J. Yang, X. Hou, G. Li, L. Wang, N. Bai, M. Cai, L. Zhao, Y. Wang, J. Zhang, K. Chen, X. Wu, C. Yang, Y. Dai, Z. Zhang, C.F. Guo, Highly stable flexible pressure sensors with a quasi-homogeneous composition and interlinked interfaces, *Nat. Commun.* 13 (2022) 1317. https://doi.org/10.1038/s41467-022-29093-y.

[7] R. Lin, H.-J. Kim, S. Achavananthadith, Z. Xiong, J.K.W. Lee, Y.L. Kong, J.S. Ho, Digitally-embroidered liquid metal electronic textiles for wearable wireless systems, *Nat. Commun.* 13 (2022) 2190. https://doi.org/10.1038/s41467-022-29859-4.

[8] S.A. Han, M. Naqi, S. Kim, J.H. Kim, All-day wearable health monitoring system, *EcoMat* 4 (2022) e12198. https://doi.org/10.1002/eom2.12198.

[9] Z. Ma, Q. Huang, Q. Xu, Q. Zhuang, X. Zhao, Y. Yang, H. Qiu, Z. Yang, C. Wang, Y. Chai, Z. Zheng, Permeable superelastic liquid-metal fibre mat enables biocompatible and monolithic stretchable electronics, *Nat. Mater.* 20 (2021) 859-868. https://doi.org/10.1038/s41563-020-00902-3.

[10] Q. Zhuang, Z. Ma, Y. Gao, Y. Zhang, S. Wang, X. Lu, H. Hu, C. Cheung, Q. Huang, Z. Zheng, Liquid–Metal-Superlyophilic and Conductivity–Strain-Enhancing Scaffold for Permeable Superelastic Conductors, *Adv. Funct. Mater.* 31 (2021) 2105587. https://doi.org/10.1002/adfm.202105587.

[11] Y. Leterrier, Durability of nanosized oxygen-barrier coatings on polymers, *Prog. Mater. Sci.* 48 (2003) 1-55. https://doi.org/10.1016/S0079-6425(02)00002-6.

[12] K.D. Harris, A.L. Elias, H.J. Chung, Flexible electronics under strain: a review of mechanical characterization and durability enhancement strategies, *J. Mater. Sci.* 51 (2015) 2771-2805. https://doi.org/10.1007/s10853-015-9643-3.

[13] K. Chae, V.T. Nguyen, S. Lee, T.Q. Phung, Y. Sim, M.-J. Seong, S. Lee, Y.H. Ahn, S. Lee, S. Ryu, J.-Y. Park, Mechanical failures of Two-Dimensional materials on polymer substrates, *Appl. Surf. Sci.* 605 (2022) 154736.

https://doi.org/10.1016/j.apsusc.2022.154736.

[14] O. Glushko, P. Kraker, M.J. Cordill, Explicit relationship between electrical and topological degradation of polymer-supported metal films subjected to mechanical loading, *Appl. Phys. Lett.* 110 (2017) 191904. https://doi.org/10.1063/1.4982802.

[15] S. Han, B.-K. Ju, C. Yang, Ultra-flexible and transparent electrodes with controllable crack length via metal–polymer hybrid nanostructure, *Thin Solid Films* 757 (2022) 139388. https://doi.org/10.1016/j.tsf.2022.139388.

[16] F. Wu, Y. Liu, J. Zhang, S. Duan, D. Ji, H. Yang, Recent Advances in High-Mobility and High-Stretchability Organic Field-Effect Transistors: From Materials, Devices to Applications, *Small Methods* 5 (2021) 2100676. https://doi.org/10.1002/smtd.202100676.

[17] R. Wang, E. Tang, G. Yang, Y. Han, C. Chen, Dynamic fracture behavior of piezoelectric ceramics under impact: Force-electric response and electrical breakdown, *J. Eur. Ceram. Soc.* 41 (2021) 139-150. https://doi.org/10.1016/j.jeurceramsoc.2021.05.021.

[18] C. Cho, P. Kang, A. Taqieddin, Y. Jing, K. Yong, J.M. Kim, M.F. Haque, N.R. Aluru, S. Nam, Strain-resilient electrical functionality in thin-film metal electrodes using two-dimensional interlayers, *Nat. Electron.* 4 (2021) 126-133. https://doi.org/10.1038/s41928-021-00538-4.

[19] P. Li, Y. Zhang, Z. Zheng, Polymer-Assisted Metal Deposition (PAMD) for Flexible and Wearable Electronics: Principle, Materials, Printing, and Devices, *Adv. Mater.* 31 (2019) 1902987. https://doi.org/10.1002/adma.201902987.

[20] Y. Yu, X. Xiao, Y. Zhang, K. Li, C. Yan, X. Wei, L. Chen, H. Zhen, H. Zhou, S. Zhang, Z. Zheng, Photoreactive and Metal-Platable Copolymer Inks for High-Throughput, Room-Temperature Printing of Flexible Metal Electrodes for Thin-Film Electronics, *Adv. Mater.* 28 (2016) 4926-34. https://doi.org/10.1002/adma.201505119.

[21] P. Kowol, S. Bargmann, P. Görrn, J. Wilmers, Strain relief by controlled cracking in highly stretchable multi-layer composites, *Extreme Mech. Lett.* 54 (2022) 101724. https://doi.org/10.1016/j.eml.2022.101724.

[22] H. Hu, X. Guo, Y. Zhang, Z. Chen, L. Wang, Y. Gao, Z. Wang, Y. Zhang, W. Wang, M. Rong, G. Liu, Q. Huang, Y. Zhu, Z. Zheng, Elasto-Plastic Design of Ultrathin Interlayer for Enhancing Strain Tolerance of Flexible Electronics, *ACS Nano* 17 (2023) 3921-3930. https://doi.org/10.1021/acsnano.2c12269.

[23] K.H. Nam, I.H. Park, S.H. Ko, Patterning by controlled cracking, *Nature* 485 (2012) 221-224. https://doi.org/10.1038/nature11002.

[24] M. Liu, S. Yu, L. He, Y. Ni, Recent progress on crack pattern formation in thin films, *Soft Matter* 18 (2022) 5906-5927. https://doi.org/10.1039/D2SM00716A.

[25] M. Kim, D. Ha, T. Kim, Cracking-assisted photolithography for mixed-scale patterning and nanofluidic applications, *Nat. Commun.* 6 (2015) 6247. https://doi.org/10.1038/ncomms7247.

[26] Q. Zhao, H. Yang, B. Nie, Y. Luo, J. Shao, G. Li, Wafer-Scale and Cost-Effective Manufacturing of Controllable Nanogap Arrays for Highly Sensitive SERS Sensing, *ACS Appl. Mater. Interfaces* 14 (2022) 3580-3590. https://doi.org/10.1021/acsami.1c22465.

[27] Q. Zhao, J. Shao, H. Tian, X. Li, C. Wang, J. Liu, Batch fabrication of nanogap electrodes arrays with controllable cracking for hydrogen sensing, *Sens. Actuator B-Chem.* 270 (2018) 475-481. https://doi.org/10.1016/j.snb.2018.05.072.

[28] C. Zhang, J. Sun, Y. Lu, J. Liu, Nanocrack-based strain sensors, *J. Mater. Chem. C* 9 (2021) 754-772. https://doi.org/10.1039/D0TC04346J.

[29] Z. Liu, D. Qi, P. Guo, Y. Liu, B. Zhu, H. Yang, Y. Liu, B. Li, C. Zhang, J. Yu, B. Liedberg, X. Chen, Thickness-Gradient Films for High Gauge Factor Stretchable Strain Sensors, *Adv. Mater.* 27 (2015) 6230-6237. https://doi.org/10.1002/adma.201503288.

[30] M. Zhu, S. Ji, Y. Luo, F. Zhang, Z. Liu, C. Wang, Z. Lv, Y. Jiang, M. Wang, Z. Cui, G. Li, L. Jiang, Z. Liu, X. Chen, A Mechanically Interlocking Strategy Based on Conductive Microbridges for Stretchable Electronics, *Adv. Mater.* 34 (2022) 2101339. https://doi.org/10.1002/adma.202101339.

[31] T. Zhu, K. Wu, Y. Xia, C. Yang, J. Chen, Y. Wang, J. Zhang, X. Pu, G. Liu, J. Sun, Topological Gradients for Metal Film-Based Strain Sensors, *Nano Lett.* 22 (2022) 6637-

6646. https://doi.org/10.1021/acs.nanolett.2c01967.

[32] D. Kang, P.V. Pikhitsa, Y.W. Choi, C. Lee, S.S. Shin, L. Piao, B. Park, K.-Y. Suh, T.-i. Kim, M. Choi, Ultrasensitive mechanical crack-based sensor inspired by the spider sensory system, *Nature* 516 (2014) 222-226. https://doi.org/10.1038/nature14002.

[33] X. Chen, Q. Zeng, J. Shao, S. Li, X. Li, H. Tian, G. Liu, B. Nie, Y. Luo, Channel-Crack-Designed Suspended Sensing Membrane as a Fully Flexible Vibration Sensor with High Sensitivity and Dynamic Range, *ACS Appl. Mater. Interfaces* 13 (2021) 34637-34647. https://doi.org/10.1021/acsami.1c09963.

[34] X.F. Zhu, B. Zhang, J. Gao, G.P. Zhang, Evaluation of the crack-initiation strain of a Cu–Ni multilayer on a flexible substrate, *Scripta Mater.* 60 (2009) 178-181. https://doi.org/10.1016/j.scriptamat.2008.10.004.

[35] H.R. Choi, S.K. Eswaran, S.M. Lee, Y.S. Cho, Enhanced Fracture Resistance of Flexible ZnO:Al Thin Films in Situ Sputtered on Bent Polymer Substrates, *ACS Appl. Mater. Interfaces* 7 (2015) 17569-17572. https://doi.org/10.1021/acsami.5b04727.

[36] N. Lu, Z. Suo, J.J. Vlassak, The effect of film thickness on the failure strain of polymer-supported metal films, *Acta Mater.* 58 (2010) 1679-1687. https://doi.org/10.1016/j.actamat.2009.11.010.

[37] X. Zhu, B. Zhang, J. Gao, G. Zhang, Evaluation of the crack-initiation strain of a Cu–Ni multilayer on a flexible substrate, *Scripta Mater.* 60 (2009) 178-181. https://doi.org/10.1016/j.scriptamat.2008.10.004.

[38] R.M. Niu, G. Liu, C. Wang, G. Zhang, X.D. Ding, J. Sun, Thickness dependent critical strain in submicron Cu films adherent to polymer substrate, *Appl. Phys. Lett.* 90 (2007) 161907. https://doi.org/10.1063/1.2722684.

[39] C. Peng, Z. Jia, D. Bianculli, T. Li, J. Lou, In situ electro-mechanical experiments and mechanics modeling of tensile cracking in indium tin oxide thin films on polyimide substrates, *J. Appl. Phys.* 109 (2011) 103530. 10.1063/1.3592341.

[40] M. Amer, Q. Hayat, V. Janik, N. Jennett, J. Nottingham, M. Bai, A Review on In Situ Mechanical Testing of Coatings, *Coatings* 12 (2022) 299. https://doi.org/10.3390/coatings12030299.

[41] N. Lu, X. Wang, Z. Suo, J. Vlassak, Metal films on polymer substrates stretched beyond 50%, *Appl. Phys. Lett.* 91 (2007) 221909. https://doi.org/10.1063/1.2817234.

[42] O. Glushko, B. Putz, M.J. Cordill, Determining effective crack lengths from electrical measurements in polymer-supported thin films, *Thin Solid Films* 699 (2020) 137906. https://doi.org/10.1016/j.tsf.2020.137906.

[43] Z. Chai, Y. Liu, X. Lu, D. He, Reducing adhesion force by means of atomic layer deposition of ZnO films with nanoscale surface roughness, *ACS Appl. Mater. Interfaces* 6 (2014) 3325-30. https://doi.org/10.1021/am4053333.

[44] Z. Suo, E.Y. Ma, H. Gleskova, S. Wagner, Mechanics of rollable and foldable film-on-foil electronics, *Appl. Phys. Lett.* 74 (1999) 1177-1179. 10.1063/1.123478.

[45] A.M.A. Talab, Z. Huang, F. Xi, L. HaiMing, Detection crack in image using Otsu method and multiple filtering in image processing techniques, *Optik* 127 (2016) 1030-1033. https://doi.org/10.1016/j.ijleo.2015.09.147.

[46] I. Ben Cheikh, G. Parry, D. Dalmas, R. Estevez, J. Marthelot, Analysis of the multi-cracking mechanism of brittle thin films on elastic-plastic substrates, *Int. J. Solids Struct.* 180-181 (2019) 176-188. https://doi.org/10.1016/j.ijsolstr.2019.07.026.

[47] J. Li, C. Li, L. Li, Q. Wang, Z. Wang, S. Wang, C. Sun, Study on fracture behavior in stiff-thin-film-on-soft-substrate structures under biaxial stress state, *Int. J. Solids Struct.* 219-220 (2021) 51-62. https://doi.org/10.1016/j.ijsolstr.2021.03.005.

[48] S.V. Shinde, S. Sampath, Interplay between cracking and delamination in incrementally deposited plasma sprayed coatings, *Acta Mater.* 215 (2021) 117074. https://doi.org/10.1016/j.actamat.2021.117074.

[49] A. Pineau, A.A. Benzerga, T. Pardoen, Failure of metals I: Brittle and ductile fracture, *Acta Mater.* 107 (2016) 424-483. https://doi.org/10.1016/j.actamat.2015.12.034.

[50] M. Moriyama, K. Matsunaga, M. Murakami, The effect of strain on abnormal grain growth in Cu thin films, *J. Electron. Mater.* 32 (2003) 261-267. https://doi.org/10.1007/s11664-003-0219-7.

[51] J.-H. Kim, A. Nizami, Y. Hwangbo, B. Jang, H.-J. Lee, C.-S. Woo, S. Hyun, T.-S.

Kim, Tensile testing of ultra-thin films on water surface, *Nat. Commun.* 4 (2013) 2520. https://doi.org/10.1038/ncomms3520.

[52] M.H. Zhao, R. Fu, D. Lu, T.Y. Zhang, Critical thickness for cracking of Pb(Zr0.53Ti0.47)O3 thin films deposited on Pt/Ti/Si(100) substrates, *Acta Mater.* 50 (2002) 4241-4254. https://doi.org/10.1016/S1359-6454(02)00254-9.

[53] A. Mora, K.A. Khan, T. El Sayed, Prediction of crack density and electrical resistance changes in indium tin oxide/polymer thin films under tensile loading, *Int. J. Damage Mech.* 24 (2015) 546-561. https://doi.org/10.1177/1056789514539362.

[54] B. Park, J. Kim, D. Kang, C. Jeong, K.S. Kim, J.U. Kim, P.J. Yoo, T.-i. Kim, Dramatically Enhanced Mechanosensitivity and Signal-to-Noise Ratio of Nanoscale Crack-Based Sensors: Effect of Crack Depth, *Adv. Mater.* 28 (2016) 8130-8137. https://doi.org/10.1002/adma.201602425.

[55] T. Li, Z.Y. Huang, Z.C. Xi, S.P. Lacour, S. Wagner, Z. Suo, Delocalizing strain in a thin metal film on a polymer substrate, *Mech. Mater.* 37 (2005) 261-273. https://doi.org/10.1016/j.mechmat.2004.02.002.

[56] R.L. Kovács, S. Gyöngyösi, G. Langer, E. Baradács, L. Daróczi, P. Barkóczy, Z. Erdélyi, Effect of nanoscopic defects on barrier performance of thin films deposited by plasma-enhanced atomic layer deposition on flexible polymers, *Thin Solid Films* 738 (2021) 138960. https://doi.org/10.1016/j.tsf.2021.138960.

[57] A. Srivastava, L. Ponson, S. Osovski, E. Bouchaud, V. Tvergaard, A. Needleman, Effect of inclusion density on ductile fracture toughness and roughness, *J. Mech. Phys. Solids* 63 (2014) 62-79. https://doi.org/10.1016/j.jmps.2013.10.003.

[58] Z. Jia, T. Li, Necking limit of substrate-supported metal layers under biaxial in-plane loading, *Int. J. Plast.* 51 (2013) 65-79. https://doi.org/10.1016/j.ijplas.2013.06.007.